BNL-113796-2017-JA

Theor Appl Climatol (2017) 127:627–642
DOI 10.1007/s00704-015-1648-y

ORIGINAL PAPER

Quantifying the local influence at a tall tower site in nocturnal conditions

David Werth[1] · Robert Buckley[1] · Gengsheng Zhang[2] · Robert Kurzeja[1] · Monique Leclerc[2] · Henrique Duarte[2] · Matthew Parker[1] · Thomas Watson[3]

Received: 20 August 2014 / Accepted: 24 September 2015 / Published online: 17 October 2015

Abstract The influence of the local terrestrial environment on nocturnal atmospheric CO_2 measurements at a 329-m television transmitter tower (and a component of a CO_2 monitoring network) was estimated with a tracer release experiment and a subsequent simulation of the releases. This was done to characterize the vertical transport of emissions from the surface to the uppermost tower level and how it is affected by atmospheric stability. The tracer release experiment was conducted over two nights in May of 2009 near the Department of Energy's Savannah River Site (SRS) in South Carolina. Tracer was released on two contrasting nights—slightly stable and moderately stable—from several upwind surface locations. Measurements at the 329-m level on both nights indicate that tracer was able to mix vertically within a relatively short (~24 km) distance, implying that nocturnal stable conditions do not necessarily prevent vertical dispersion in the boundary layer and that CO_2 measurements at the tower are at least partly influenced by nearby emissions. A simulation of the tracer release is used to calculate the tower footprint on the two nights to estimate the degree to which the local domain affects the tower readings. The effect of the nocturnal boundary layer on the area sampled by the tower can be seen clearly, as the footprints were affected by changes in stability. The contribution of local sources to the measurements at the tower was minimal, however, suggesting that nocturnal concentrations at upper levels are contributed mostly by regional sources.

✉ David Werth
david.werth@srnl.doe.gov

[1] Savannah River National Laboratory, Building 773-A, Aiken, SC 29808, USA

[2] Laboratory for Atmospheric and Environmental Physics, University of Georgia, Griffin, GA, USA

[3] Tracer Technology Group, Brookhaven National Laboratory, Upton, NY, USA

1 Introduction

In contrast with the multitude of studies of vertical transport in the convective boundary layer (e.g., Wang et al. 2007; Barkhatov et al. 2012), vertical transport modeling and measurements remain scarce in the stable boundary layer (Sogachev and Leclerc 2011). This lack of robust data can hinder the interpretation of gas concentration measurements made at a tall tower sensor under stable conditions. Networks of towers are currently employed as platforms for making CO_2 measurements, with the goal of constraining global-scale carbon budgets (Andrews et al. 2013). Concentrations at a single tall (> 300 m) tower should be representative of continental-scale CO_2 distributions (Desai et al. 2008), but the surface area over which emissions are detected at an upper tower level is dictated by the local meteorology, especially the atmospheric stability (Gerbig et al. 2009; Sogachev and Leclerc 2011; Gloor et al. 2001). Stable conditions often prevail during nighttime, making such periods ideal for continental-scale sampling (Gloor et al. 2001). Nocturnal turbulent conditions do occur, however, depending on the local terrain and meteorology, and the sampled area will tend to be local if there is significant vertical mixing of respired CO_2 (Gerbig et al. 2009). In their paper on continental carbon exchange, Gerbig et al. (2009) describe the issues involved in the design and interpretation of a tower network and write "In a network of tall towers, the most important [question] is to ask: 'what is it that the individual tower observes?'". We need to know more about nocturnal eddy transport and the influence of the nearby environment on a tower.

The area sampled by a tower in any particular condition is often described by its "footprint," a function that weights the contribution from each point at the surface to the measured signal (Schmid 2002; Gerbig et al. 2009; Sogachev and Leclerc 2011; Barcza et al. 2009; Chen et al. 2013). The calculation of a footprint is often accomplished with a transport model that uses as input either a meteorological reanalysis (Gloor et al. 2001; Gerbig et al. 2009; Hegarty et al. 2013) or data from a boundary layer model (Sogachev and Leclerc 2011). As the planetary boundary layer (PBL) becomes more turbulent, the footprint will be confined to an area near the tower as vertical mixing will quickly move CO_2 upwards. Gerbig et al. (2009), for example, used the Stochastic Time-Inverted Lagrangian Transport (STILT) transport model with an analyzed wind field to estimate footprints of the 30-m level of the Harvard Forest tower in turbulent daytime conditions (when mixing leads to small differences between the 30- and 300-m levels) and noted the dominant influence within 20 km of the tower. In stable conditions, however, the footprint should begin at a surface point well away from the tower and extend for long distances (Sogachev and Leclerc 2011).

In August 2008, the "South Carolina Tower" (SCT), a 329-m television transmitter tower near Beech Island, SC, was incorporated into the National Oceanic and Atmospheric Administration's (NOAA) tall tower network (a subset of the Ameriflux network), which measures carbon concentrations to quantify the terms of the global carbon flux, especially those dealing with the land surface (Birdsey et al. 2009; Stephens et al. 2007; Gourdji et al. 2012). Terrestrial ecosystems constitute a major sink of carbon, but their magnitude is uncertain (Birdsey et al. 2009). NOAA initiated the Carbon Tracker project to process global carbon measurements and produce a complete global carbon budget (Peters et al. 2007). The tower network is currently active in making measurements (Andrews et al. 2013), and this monitoring resource forms the North American backbone of the Carbon Tracker project.

Our goal is to determine the location of sources contributing to the flux signature measured at the SCT. The objective of this project is to obtain detailed information about the way eddy activity acts to move a gas emitted from the surface near the SCT upward to higher levels in the absence of convection. To accomplish this, a set of artificial tracers was released into the nocturnal boundary layer (NBL) on two nights from various locations within a 24-km distance upwind of the tower (Parker et al., in preparation) and time series of tracer concentrations at three tower levels were recorded. The source area around a tower can be characterized by a "near field" (within ~50 km) and a "far field" out to the order of 1000 km (Gerbig et al. 2009), and the focus here is on the SCT near field. Therefore, a high-resolution mesoscale PBL simulation of a 19 km × 26 km domain (encompassing the area of the experiment) is coupled to a transport model of the tracer release and validated against the tracer signal at the tower. The coupled model is then used to estimate the footprints on the two nights.

Several experiments and simulations have helped elucidate vertical dispersion in the non-convective environment. Pasquill and Smith (1983) describe several tracer release field experiments done under neutral and stable conditions, measuring the vertical distribution at towers within the range of 230 m. Sogachev and Leclerc (2011) applied the Scalar Distribution (SCADIS) boundary layer model with a Lagrangian transport model to estimate footprints in the stable boundary layer, and they found that "the changing atmospheric stratification determines the footprint which depends not only on the height of a sensor but also on the time of measurements." They also note that the calculation of a footprint can be made more robust with the inclusion of actual data for comparison, and this is the goal of the current research. With a validated simulation of tracer transport, the plume behavior and tower footprint in stable and neutral conditions can be quantified, allowing us to understand better the degree to which the SCT is influenced by the local environment.

2 Tracer field experiment

Tracer releases are a well-established method to study atmospheric motions (van Dop et al. 1998; Leclerc et al. 2003a, b), but their use to study stable boundary layers is less common. A nocturnal tracer study was conducted at the SCT site in May 2009 (Parker et al. in preparation), with the goal of evaluating the way gas released from the area near the tall tower is mixed upward into the moderately stable or slightly stable boundary layer during lateral advection. The experiment comprised the released tracers and their detection at various heights on the SCT, and the data was then used to validate a simulation of the release. The tracer release was conducted on each of two nights, a slightly stable night (May 11th/12th, 2009, "night 1") and a second, moderately stable night (May 12th/13th, 2009, "night 2"), identified as such by their temperature profiles, the values of the friction velocity (u^*), and Vaisala CL31 (Helsinki, Finland) lidar ceilometer readings of the boundary layer height. Compared to night 1, night 2 has a stronger late-night inversion (Fig. 1a), lower u^* values (Fig. 1b) (especially at 329 m), and a shallower mixing layer (Fig. 1c). On night 1, the u^* values fall after peaking at around 0700 UTC (3:00 am EDT), while the values on night 2 rise after reaching a minimum at around the same time (despite a falling boundary layer height (Fig. 1c)). This occurs during the release of the tracers and will affect tracer behavior differently on the two nights. Selected tracer data from this field experiment and local meteorological measurements are used in this study (Parker et al., in preparation).

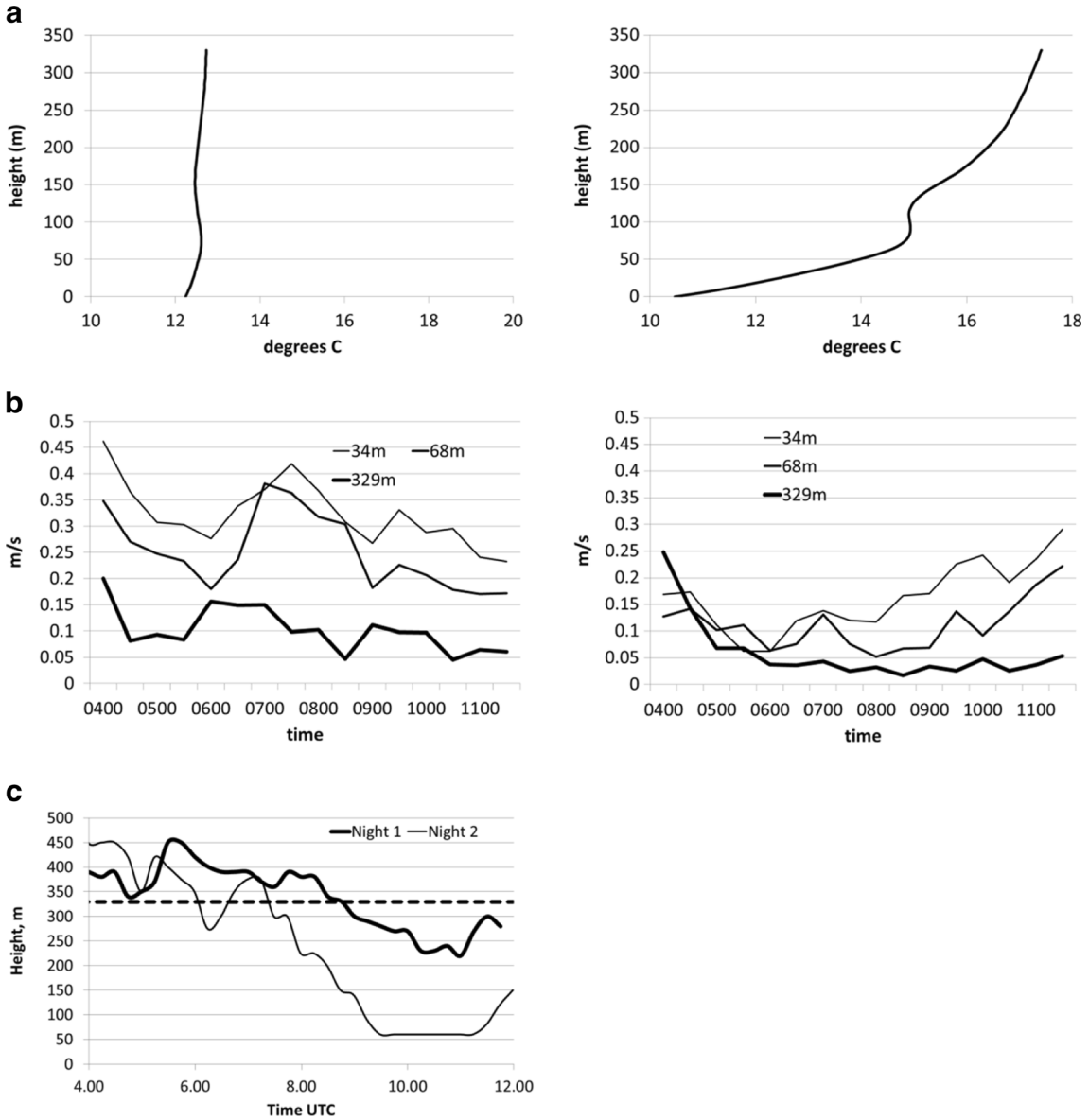

Fig. 1 **a** Radio Acoustic Sounding System (RASS) temperature sounding at 6:00 am EDT (1000 UTC) for (*left*) May 11/12th (night 1), (*right*) May 12/13th (night 2), **b** as in **a** but for the time series of u^* calculated at the three tower levels. **c** LIDAR ceilometer readings of the boundary layer height for both nights. The *dotted line* is at 329 m

2.1 Materials and methods

The SCT site is located within a region characterized by broken forests and agriculture in the immediate vicinity, with suburban, urban, and industrial areas (most notably Augusta, GA) within 20 km. A set of release points was established from about 3 to 24 km in the quadrant northeast of the SCT, which was equipped with sampling tubes. As part of the overall experiment, perfluorocarbon tracer Perfluorotrimethylcyclohexane (PTCH) (molecular weight = 450 g/mol) was released at ground level from two distant points near Aiken, SC, designated as WA (night 1) and UE (night 2) (Fig. 2). This tracer has a background concentration of several parts per quadrillion by volume (Parker et al., in preparation), so we expect an unambiguous signal at the tower. The PTCH tracer release began at 2:00 am EDT (0600 UTC) on each night. Tracer release ended at 6:00 am EDT (1000 UTC) on night 1, while ending at 5:15 am EDT (0915 UTC) on night 2. This means that the tracer release occurred during the period of large u^* values on night 1 (Fig. 1b, left), during the lower (but rising) u^* values on night 2 (Fig. 1b, right), and during the period of gradual stabilization on both nights (Fig. 1c).

The tall tower is normally equipped with several types of sensors—a (NOAA) tube sampler for CO_2, an open-path infrared gas analyzer for CO_2 and water vapor (Licor Model 7500), and a sonic anemometer (ATI Model S_a, ATI Model S_x) to measure the three-dimensional wind components and, through its measurements of wind speed variability, virtual

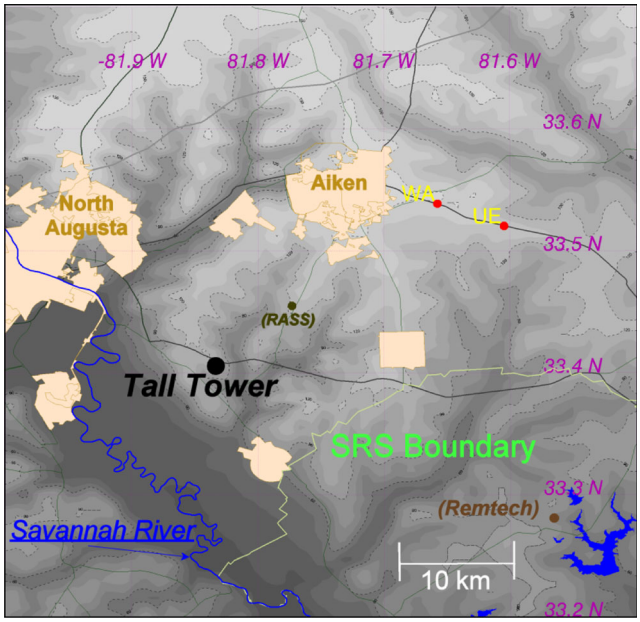

Fig. 2 Map of tracer release points (*red*) as well as the tower receptor (*black*). Topographic heights range from 30 m above sea level (*darkest shading*) to 150 m (*lightest shading*)

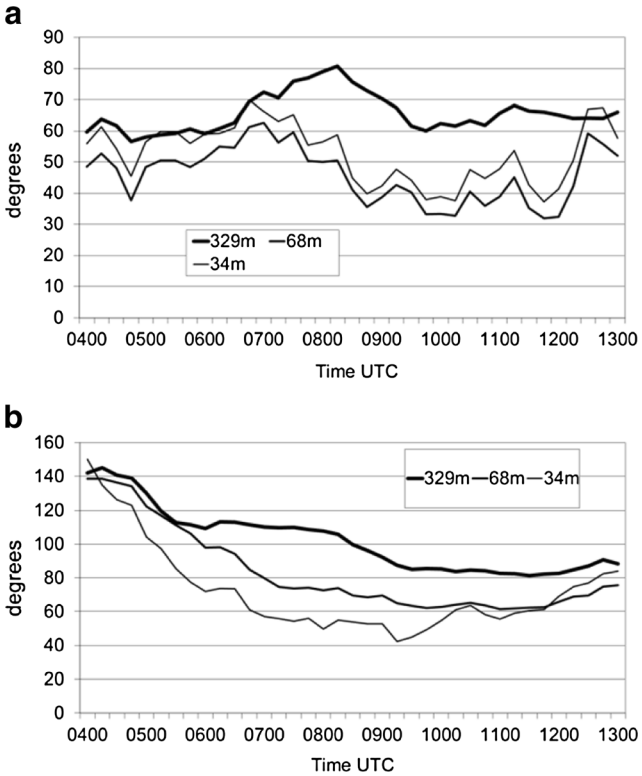

Fig. 3 Wind direction (°) at Tall Tower on **a** night 1 and **b** night 2

temperature. For the tracer release experiment, an additional tube sampler was added to measure PTCH concentrations. The sensors and tube sampler inlets are deployed at three levels: 34, 68, and 329 m. The tube samplers have been discussed in Parker et al. (in preparation), and the reader is referred there for a detailed description.

In addition to the tower data, a sodar with a radio acoustic sounding system (RASS) extension (Scintec AG, model SFAS, Rottenburg, Germany) was installed at 33.455 N, 81.7739 W, near the center of the experiment domain (Fig. 2), providing temperature and three-dimensional components of the velocity and boundary layer depth at 5 m resolution up to 300 m (Parker et al., in preparation). A second sodar (Remtech PA2) was installed at 33.340 N, 81.564 W (Fig. 2), providing another source of wind data throughout the depth of the boundary layer.

2.2 Experimental results

2.2.1 Night 1: 11 to 12 May, 2009—slightly stable case

The tower readings reveal that boundary layer winds came from the northeast quadrant the entire night at all levels (Fig. 3a), in agreement with the RASS (Fig. 4a). Winds at upper levels slowed as the night progressed (Fig. 4a). The winds at higher levels were more easterly (Fig. 3a), influenced by high pressure to the north. Downslope flow at lower levels was northeasterly, influenced by a decrease in elevation to the southwest (Fig. 2). Weak vertical temperature gradients persisted the entire night (Fig. 4c). The signal at the tower from the released tracer is represented by its χ/Q ratio—the concentration normalized by the release rate. The PTCH tracer from point WA reached the tower about 3 h after the tracer release started at 2:00 am EDT (0600 UTC) (Fig. 5a), after the 34- and 68-m winds shifted to ~45°, with values at the upper level peaking at about 1/2 of the lower level value. We also see how the upper level peak arrives later than that at the lower level, likely due to the veering wind which would cause the plume to bend clockwise at upper levels. The latter is also apparent in the sudden increase in χ/Q after 1000 UTC—no increase in turbulent mixing at this time is seen in Fig. 1b (left), implying instead that the later wind shift at upper levels (Fig. 3a) led to the sudden arrival of the plume at 329 m.

2.2.2 Night 2: 12 to 13 May, 2009—moderately stable night

On night 2, boundary layer winds started off from the southeast (Figs. 3b and 4b), forcing the tracer to the north of the tower, but shifted northward from 0400 UTC (midnight EDT) to 0900 UTC (5:00 am, EDT) (Fig. 3b), allowing for a detectable signal. We again see how topography forces the zonal wind aloft to shift northeasterly closer to the surface (Fig. 3b). A weak low-level jet (LLJ) formed at about 10:00 pm EDT (0200 UTC) (Fig. 4b), dissipated, then reformed after 5:00 am (0900 UTC). A strong inversion starts forming after 8:00 pm (0000 UTC) (Fig. 4d). As with night 1, the signal from Pt. UE arrives only after the wind shifts (Fig. 5b). This tracer was able to mix vertically before

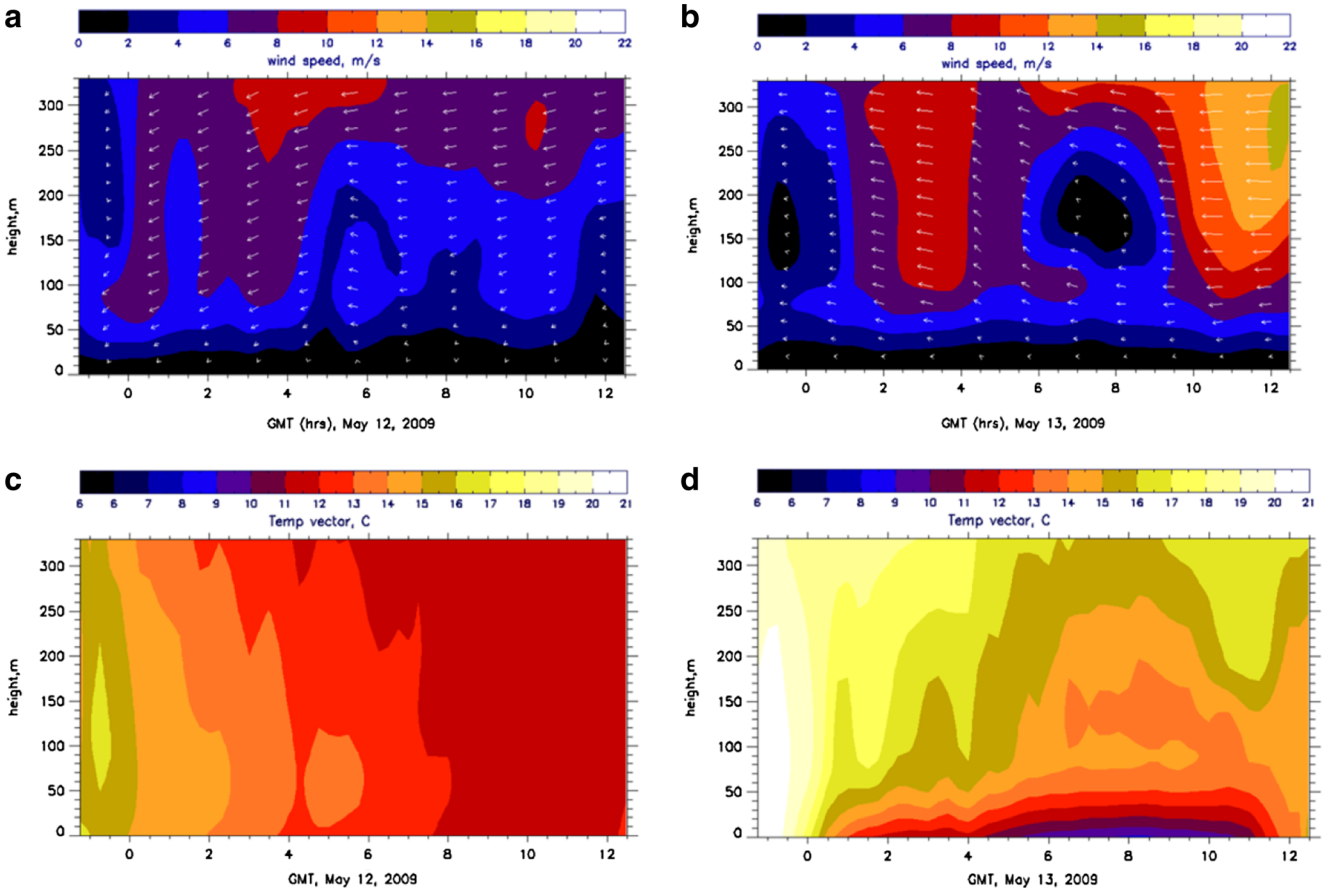

Fig. 4 Radio Acoustic Sounding System (RASS) profiles of **a** night 1 wind speed and direction, **b** night 2 wind speed and direction, **c** night 1 temperature, **d** night 2 temperature

reaching the tower (despite the low boundary layer heights present on both nights as seen in Fig. 1c), but on night 2, the most distant tracer peaks at only about 1/3 its surface value, whereas on night 1 the tracer is able to mix upward in quantities sufficient to cause the ratio of the peaks to be over half (albeit briefly), implying the vertical mixing of the tracer was weaker on the more stable second night. The 329 m χ/Q values are lower on the second night, reflecting the greater stability during this time.

3 Tracer simulation

3.1 Materials and methods

Calculating the motion of the tracer and inferring the relationship between the vertical transport and the turbulent properties of the atmosphere requires knowing the emission rate of the source as well as estimates of the advection and turbulent transport terms. While the emission rate in this study is known, modeling must be used to estimate the advection and turbulent terms. Similar to the work of Sogachev and Leclerc (2011), a meteorological model was coupled to a dispersion model to explicitly calculate the tracer concentrations at each point. Coupled dispersion simulations often lack observed concentrations of tracer for comparison to the model results (Sogachev and Leclerc 2011), but our tracer data can be used to validate our coupled simulation.

3.1.1 RAMS

The Regional Atmospheric Modeling System (RAMS, Pielke et al. 1992) has been used previously to simulate fine-scale motions within the nocturnal boundary layer (e.g., Werth et al. 2011) and is selected to recreate the meteorology from the two nights of the tracer experiment, centered over the domain in Fig. 6a. RAMS solves the non-hydrostatic equations of motion for velocity and potential temperature on a staggered polar stereographic C grid (Mesinger and Arakawa 1976). The model also employs a terrain-following sigma coordinate system in the vertical. For our purposes, an innermost domain of 200 m grid spacing was designed covering the area of the experiment (25.8 km × 19.4 km) (Fig. 6b). This grid is nested within coarser grids as described below. The Harrington radiation scheme (Harrington 1997) is applied for both shortwave and longwave radiative transfer. For convection, the Kuo

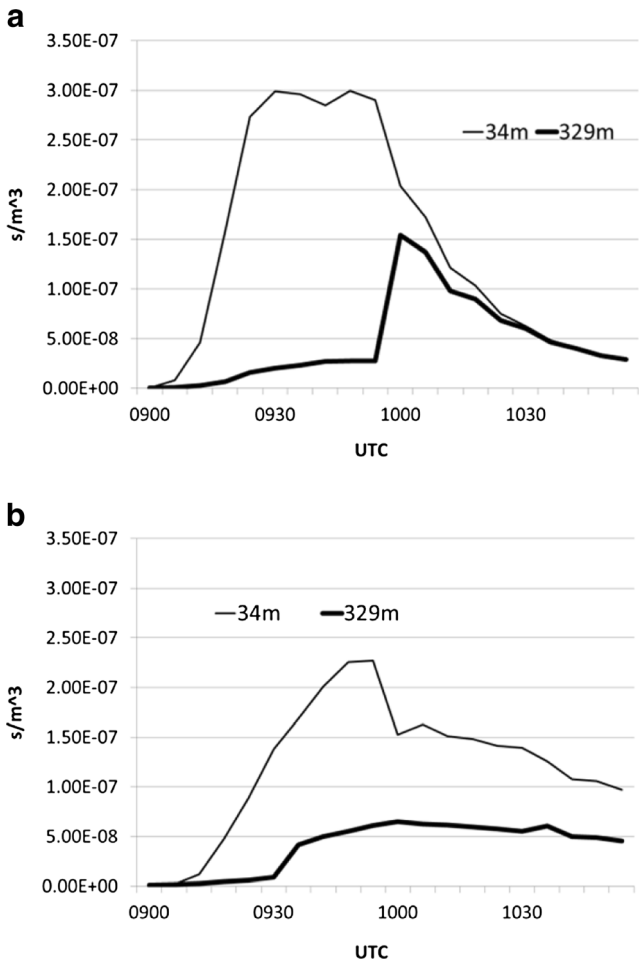

Fig. 5 χ/Q ratio for **a** night 1 and **b** night 2

scheme (Kuo 1974) is applied for the coarser grids, while the innermost, 200 m grid uses an explicit cloud prognostic scheme (Cotton et al. 1986; Meyers et al. 1992). A Newtonian "nudging" of all grids is applied, by which the outer boundary of each grid is adjusted towards the values of its parent grid (Clark and Hall 1991), with the influence of the parent gradually diminishing towards the center of the domain. Two-way nesting is applied, allowing each inner grid to in turn influence its respective parent.

The RAMS surface must be assigned values of topography and land cover, as well as an initial profile of soil energy content. For the innermost grid, the topography comes from a high-resolution (3 s) dataset (Fig. 6b), while the coarser grids use a 30-s digital elevation model dataset. Surface fluxes are calculated according to the LEAF-3 land surface scheme (Walko et al. 2000). Each grid square is partitioned into 21 land surface types, based on 1 km U.S. Geological Survey data, and the surface fluxes are calculated according to the surface variables (leaf area index, albedo, etc.) associated with each type. Each land surface type is assigned a roughness length, which is used in the PBL scheme to calculate momentum fluxes. For other initial variables, some trial and error is involved. On both nights, the initial soil energy is assigned an initial value (~1.0×10^8 J/m^3 on night 1, ~8.0×10^7 J/m^3 on night 2), higher than the observed values (~8.0×10^7 J/m^3 on night 1, ~6.5×10^7 J/m^3 on night 2), in order to more closely match the observed nocturnal boundary layers.

The model is run twice—once for the period May 11th, 2009, at 2:00 pm EDT (1800 UTC) to May 12th, 2009, at 8:00 am EDT (1200 UTC) (night 1) and again for the period May 12th, 2009, at 2:00 pm EDT (1800 UTC) to May 13th, 2009, at 8:00 am EDT (1200 UTC) (night 2). Besides the dates, several important differences exist between the two simulations. On the first night, the model is run with nested grids of 3200, 800, and 200 m, with the 13.5-km resolution Rapid Update Cycle (RUC) product used as the boundary conditions (Benjamin et al. 2004). For night 2, however, the RUC boundary dataset failed to capture the wind shift seen in Fig. 3b, requiring the use of the 32.4-km resolution North American Regional Reanalysis (which did capture it) as the boundary condition (Mesinger et al. 2004). This in turn required the addition of a new outermost grid of 12.8 km grid spacing, maintaining the 1/4 outer-to-inner ratio of grid spacing.

Another difference was in the vertical grid spacing. On night 1, the lowest level is 30 m deep, increasing 15 % for each succeeding layer up to a maximum of 500 m depth. On the more stable night 2, the lowest level was set at 15 m. On both nights, the model is run on all grids with the Mellor-Yamada scheme (Mellor and Yamada 1974) to determine eddy diffusivities in the vertical (though these were not used in the simulation of tracer dispersion), with the Smagorinsky (1963) horizontal deformation scheme for the horizontal diffusion. The latter sets diffusion equal to 0.32 multiplied by the product of the horizontal deformation and the grid spacing. On night 2, however, simulated tracer failed to mix upwards, indicating insufficient TKE. The damping term in the TKE budget equation was therefore reduced by a factor of ~17, allowing TKE to accumulate in the nocturnal boundary layer.

3.1.2 HYSPLIT

The HYbrid Single-Particle Lagrangian Integrated Trajectory (HYSPLIT) dispersion model (Draxler and Hess 1998) is applied to calculate the tracer concentration at each point in the domain, using the RAMS gridded meteorological data as input. This model has proven itself very useful for simulating airborne chemical transport from a source to a receptor location (e.g., Stunder et al. 2007) and is used here to reproduce the tracer transport from the two emission points to the SCT to be compared with the observed data. HYSPLIT is run by ingesting the RAMS data and applying a known source term, and the resulting simulated plume is then validated against the observed tracer data. The full plume simulation can then be used to elucidate the vertical tracer transport.

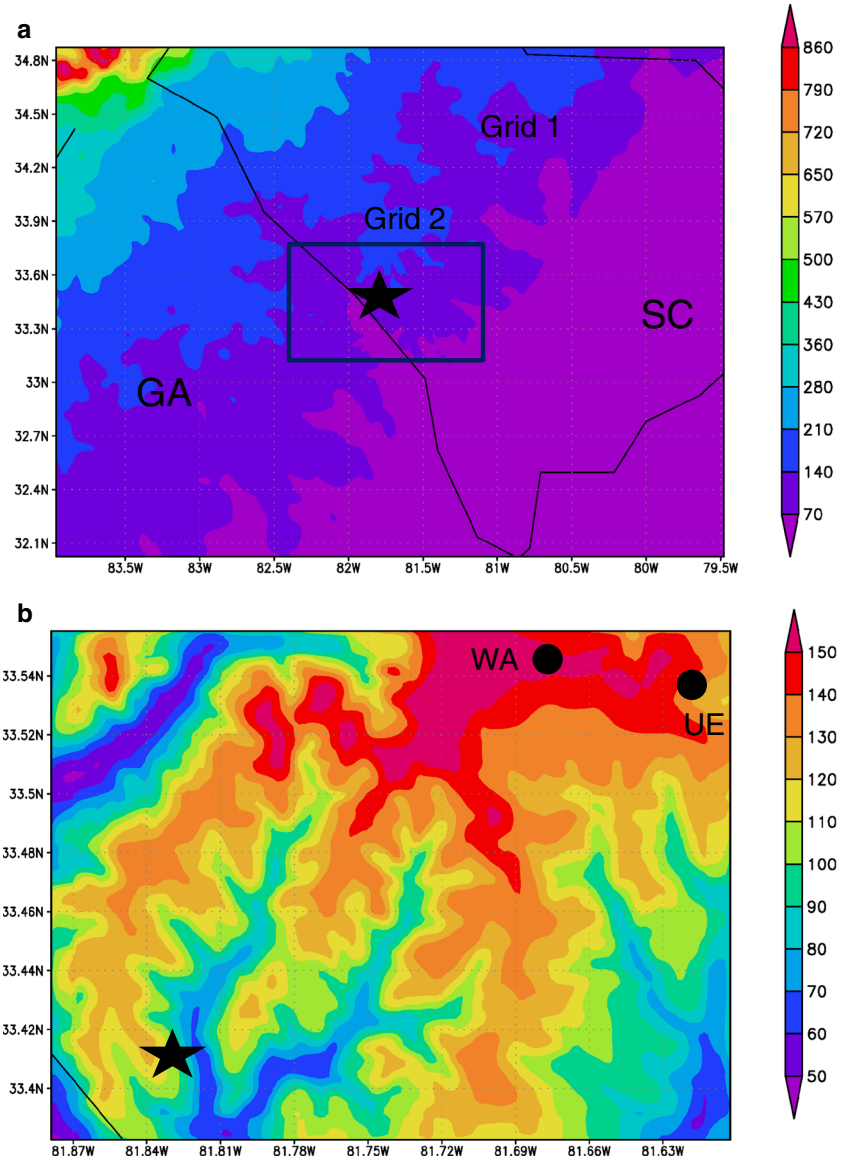

Fig. 6 Topography (m above sea level) for **a** grids 1 and 2, and **b** grid 3. The *star* indicates the tower location, and the *circles* indicate the release points

HYSPLIT uses turbulence kinetic energy (TKE) taken from the mesoscale model to calculate a Gaussian distribution of turbulent wind values, which are randomly added to the mean wind values (taken from the 200 m RAMS grid) to get the transport of each Lagrangian tracer particle. As they are released into the atmosphere, the particles will begin as a concentrated cloud that gradually disperses as the particles are assigned different turbulent velocities.

3.2 Results: night 1 (11 to 12 May, 2009)

The model wind directions and temperature on the first night (Figs. 7 and 8) approximate the observed values at two levels at the tall tower. Temperatures agree to within about 1 °C. Both levels experience a gradual cooling, with winds out of the northeast. The model captures the wind shifts and vertical shear during the night (Figs. 7c and 8c), with errors usually less than 10°. At both levels, however, the RAMS wind speeds show large errors (Figs. 7b and 8b).

The simulated PBL (Fig. 9a) and the RASS (Fig. 4a) feature winds out of the NE to ENE up to the tower level (Fig. 9a), with faster winds above 200 m from 0000 UTC (8:00 pm EDT) to 0400 UTC (midnight) that decrease afterward. Simulated cooling at the surface occurs at a slow rate (Fig. 9b), precluding the formation of an inversion in the 0–350-m range, with TKE remaining large (with a gradual decrease) within a deep layer (Fig. 9b). This has the effect of maintaining vertical turbulent transport (and preventing the LLJ from forming) throughout most of the night. We also see a weak effect of drainage flow as convergence in the

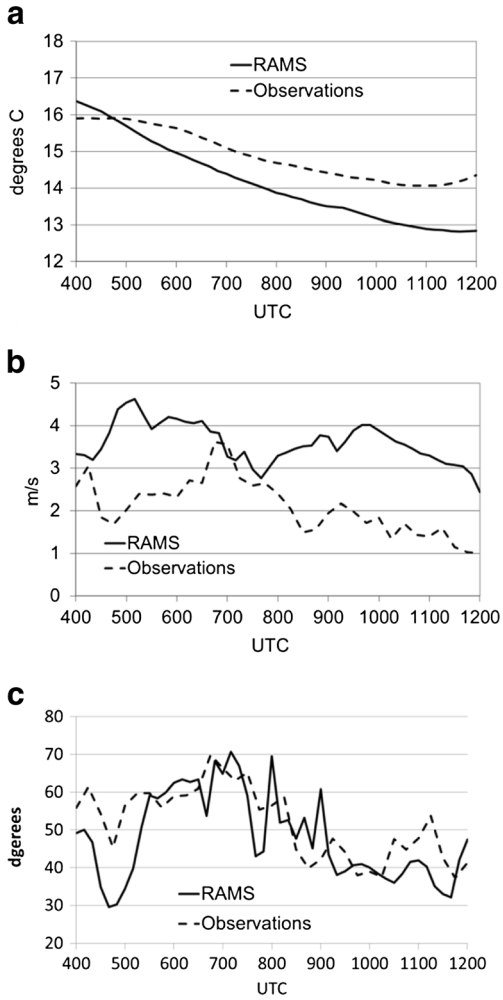

Fig. 7 Comparison of RAMS data with observed tower data for night 1 at 34 m for **a** temperature, **b** wind speed, and **c** wind direction

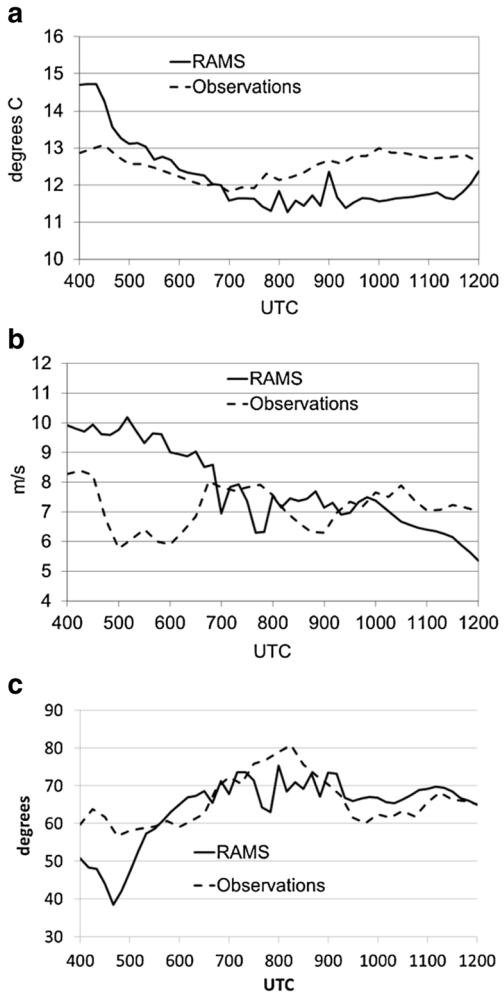

Fig. 8 As in Fig. 7 but at 329 m

low-lying areas (not shown). The observed surface loses its heat more quickly (Fig. 4c), for a more isothermal boundary layer (Fig. 4c).

The observed NBL tends to lie within the E (weakly stable) category of the Pasquill-Gifford scale (−0.5 °C/100 m < $\Delta T/\Delta z$ < 1.5 °C/100 m), with the simulated values lying in the D (neutral) category (−1.5 °C/100 m < $\Delta T/\Delta z$ < −0.5 °C/100 m), likely due to the slow cooling between 0 and 50 m. Both the simulated and the observed boundary layers are dominated by weak sinking motion (not shown), but we nevertheless expect the turbulent transport to move tracer upwards.

The meteorological variables from the RAMS simulation served as input to the HYSPLIT tracer model, and this is used to recreate what happened to the tracer that night. The release of tracer from point WA is simulated, using the known release rate (1906 g/h). We are interested in the rate at which the tracer concentrations fall with distance from the source and with height. In keeping with previous studies involving the evaluation of dispersion models against observations from field projects (Chang et al. 2003; Perry et al. 2005), we select a metric that measures the plume dispersion, the maximum tracer concentration at a fixed distance from the source, to be compared with the measured tracer maxima.

We define an arc of points that is equidistant from the release point and that intersects the tower, and look at cross-sections of the simulated plume along this arc at different times (Fig. 10a). The plume is just arriving at this distance at 0700 UTC (3:00 am EDT, 1 h after the release began), reaches its peak at 0800 UTC–0900 UTC, starts to disperse horizontally at 0900 UTC–1000 UTC, and dissipates from 1000 UTC–1100 UTC after the source is turned off (Fig. 10a). The simulated plume sweeps southward across the SCT at about 6:00 am–7:00 am EDT (1000–1100 UTC) as the wind becomes northerly. We note the shifting of the plume to the southeast, as well as the effect of directional wind shear—the upper-level peaks are often shifted relative to the lower level peak.

Errors in the simulated wind speed can cause the plume to arrive at the tower location at the wrong time, even if the

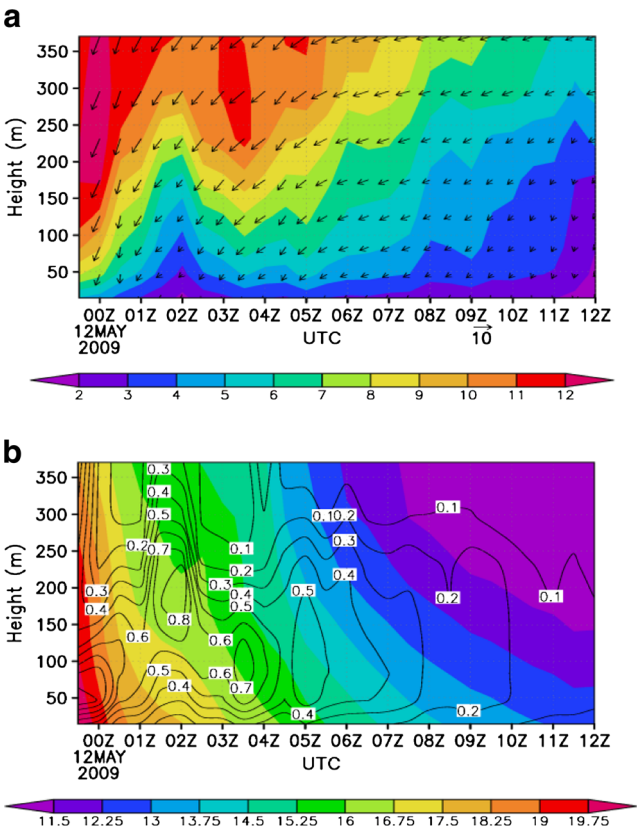

Fig. 9 **a** Simulated night 1 wind vectors and speeds (m/s) at the center of the innermost domain. **b** As in **a** but for temperature (*shaded*, °C) and TKE (m^2/s^2)

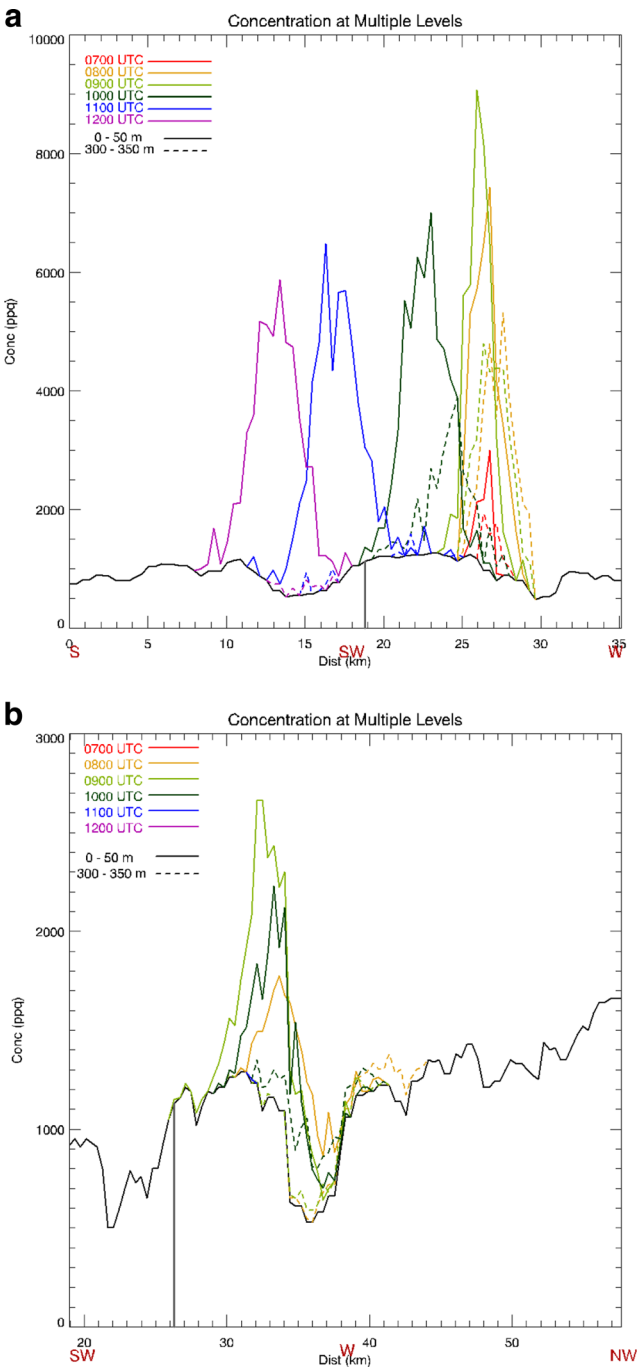

Fig. 10 Cross-section of simulated tracer concentrations as a function of distance from due south along the arc as described in the text for **a** night 1 and **b** night 2

plume forms correctly. We are interested in comparing the way that vertical mixing causes the simulated and observed plumes to vary with height. Assuming that the maximum concentration at each level represents the plume center of both the observed and actual plumes, we plot the simulated maximum value along the arc as a function of time (Fig. 11a) for comparison to the observed peaks in concentration. We see that at 34 m the simulated concentrations reach values of 8000 ppqV, similar to those seen when the actual plume swept over the tower (Fig. 11a, left). At 329 m, the simulated plume briefly reaches peak values greater than 6000 ppqV at 0830 UTC (4:30 am EDT) but starts to disperse afterwards (Fig. 11a, right). The simulated plume seems to spread out faster than the observed plume, by 1000 UTC (6:00 am, EDT); the former has dropped to 2750 ppqV, while the latter is peaking (briefly) at about 4500 ppqV before dropping to 2600 ppqV by 1020 UTC. The qualitative agreement between the two suggests that the model is simulating vertical turbulent transport with reasonable accuracy.

We next want to calculate the tower flux footprint using this simulation. The flux F at the level z_m due to a source S_o at location x_o can be described as (Hsieh et al. 2000)

$$F(z_m) = S_o f(x_o, z_m), \quad (1)$$

where f is a dimensionless flux footprint function. In a Lagrangian model, this can be approximated as

$$F(z_m) = S_o\left(n/N\right), \quad (2)$$

in which n is the number of particles that arrive at the sensor, normalized by the total number released (N) from point x_o. A series of inverse transport simulations (i.e., running the model

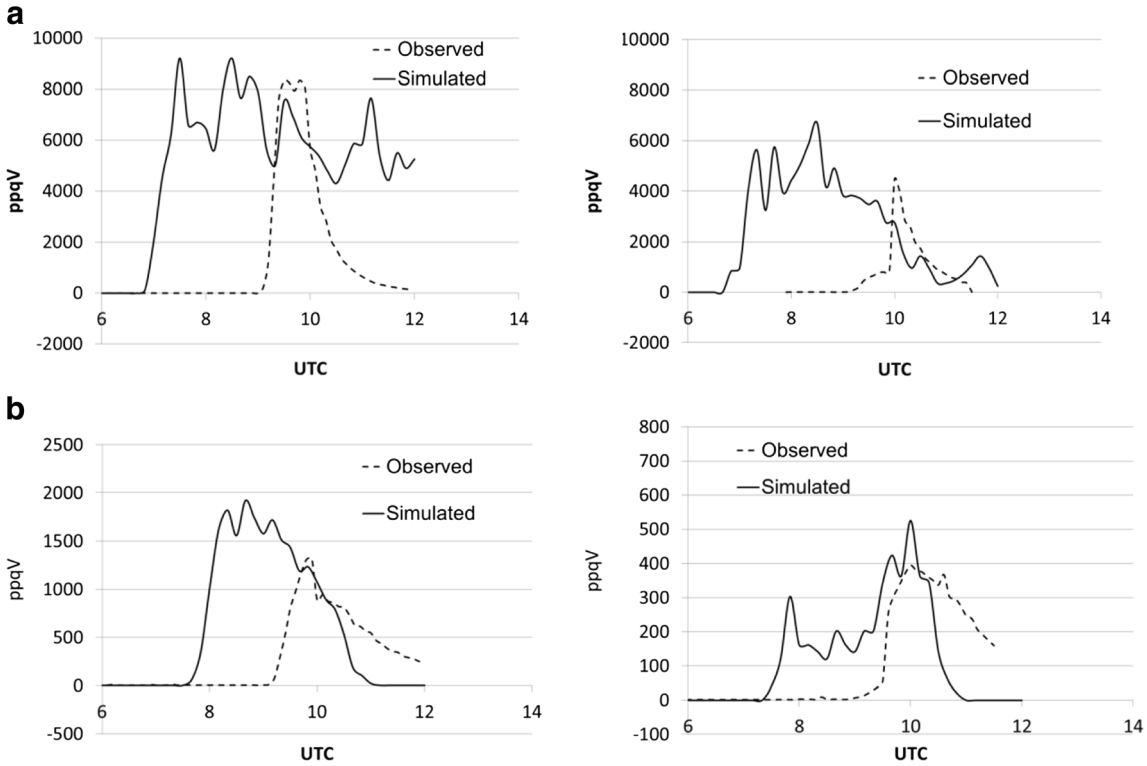

Fig. 11 **a** Time series of night 1 observed concentrations of tracer PTCH at the tower (*dashed lines*), along with the simulated maximum values along the arc (*solid lines*) at 34 m (*left*) and 329 m (*right*). **b** As in **a** but for night 2

backward in time, or "backtracking") can be performed to solve for n at any location—releasing N particles from the a level of the tower (z_m) at various times and counting how many arrive at the surface moving upwind while dispersing *downward*. This pattern of particles within the surface layer constitutes the footprint—a measure of how strongly any area near the tower contributes to the tower signal:

$$f(x_o, z_m) = n(x_o, z_m) \Big/ N, \tag{3}$$

in which $n(x_o, z_m)$ is the number that diffuses to a level near the surface from the release point of height z_m to location x_o. The more particles mix downward into a particular area, the more strongly that area influences the tower signal.

A large number of particles (N = 100,000) was released from the 329-m tower level on the grid 3 domain as a single "puff" each hour, and the fraction (n/N) of these particles that diffuses into the surface layer (0 to 20 m, approximating the level of the forest canopy) within 1 h in each model grid square constitutes the footprint (Fig. 12). (The 1-h period was chosen based on the approximate simulated travel time for the tracer to reach the distance to the tower.) On night 1, the footprint lies to the northeast of the tower at all times, a consequence of the northeasterly wind (Fig. 9). Towards the end of the period (after the actual tracer release was stopped), the footprint is reduced (Fig. 12e, f) as the TKE is reduced (Fig. 9b), implying that the local influence becomes weaker. (Note that observed u^* values fall from 0800 UTC to 1100 UTC, also implying weaker mixing.) About 50–80 % of the particles have left the domain after 1 h at all release times except for 1100 UTC, when none have. (After 2 h, however, almost no particles remain over the grid 3 domain.) Overall, the total number of particles that disperse to the 20-m level is small, falling from 3.0 % at 0600 UTC to almost zero by 1100 UTC.

An additional simulation was done in which the particles were released at 34 m, the lowest tower level. This had the effect of keeping more of the particles near the ground, but still implied a small effect of the local surface at this level; after 1 h, 2–5 % of the particles have dispersed to below 20 m, and after 2 h, very few particles (0–3 %) still within the domain are below 20 m.

3.3 Results: night 2 (12 to 13 May, 2009)

On night 2, the wind was out of the southeast as the experiment began (Fig. 3b) but swung around to the northeast during the night, providing an opportunity for the SCT to sample the plume. At 34 m, the RAMS simulation captures the wind shift and gradual rise in wind speed, as well as the gradual cooling trend (Fig. 13), though errors of about 1.0 m/s and 2° do exist,

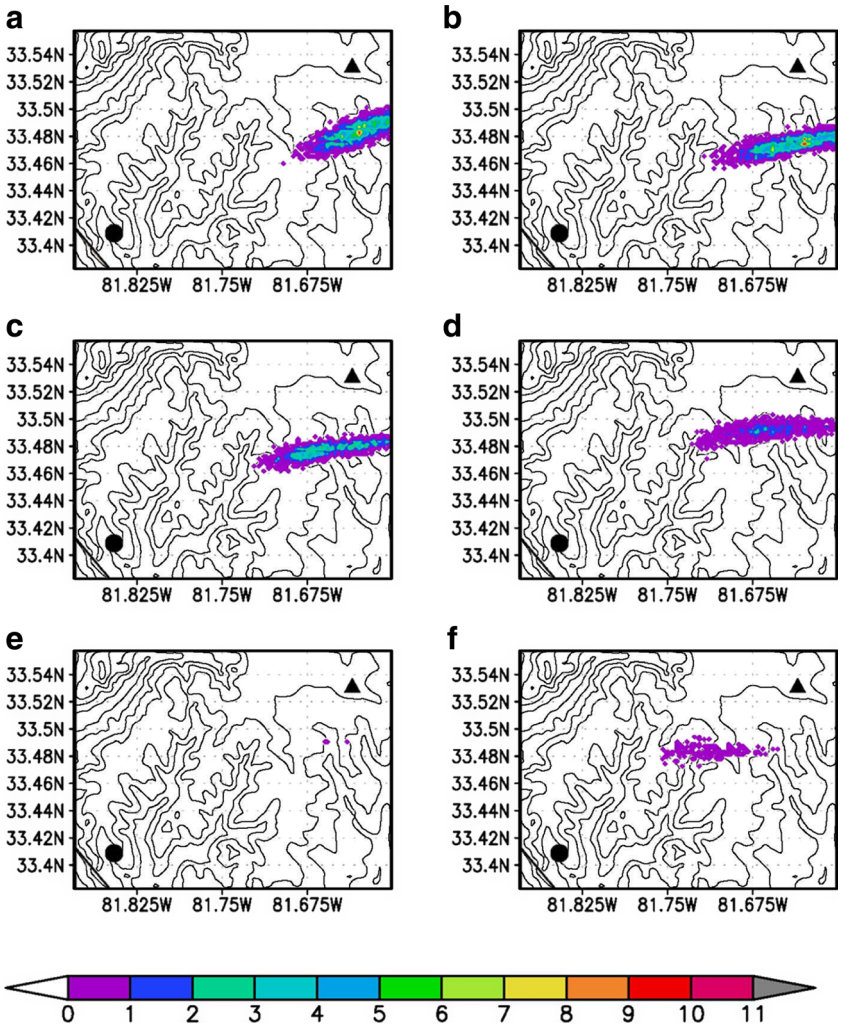

Fig. 12 Simulated night 1 footprint at landing time **a** 0600 UTC, **b** 0700 UTC, **c** 0800 UTC, **d** 0900 UTC, **e** 1000 UTC, and **f** 1100 UTC. Units represent fraction of released particles per square meter × 10^{-9}, the *dot* represents the location of the tall tower, and the *triangle* is the release point

respectively. We also see a rise of temperature after 1000 UTC (weaker in the model). At 329 m, however, the model has more difficulty with the wind speed (errors of about 3–5 m/s) and underestimates the shift in direction (errors of about 20°) (Fig. 14). We do see a weaker cooling trend at this level relative to 34 m, setting up an inversion for the later portion of the night. The simulated PBL on this night (Fig. 15) features a weak jet forming at 0300 UTC (11:00 pm EDT) that fades before reforming at 0800 UTC (4:00 am EDT), similar to the observed PBL (Fig. 4b). The strongest inversion in the model does form later than observed (Fig. 4d), and the strongest temperature gradient lies higher (between 100 and 150 m) than in the observations (at about 50 m). In the model and the observations, this night more closely resembles a classic nocturnal PBL pattern, an inversion forming late in the night, with a strong LLJ forming above it and a turbulent layer under the jet (Fig. 15b). The latter is in agreement with increased values of u^* after 0800 UTC seen in Fig. 1b (left). We also see stronger convergence in low-lying areas on night 2 (not shown), implying a stronger drainage flow on the more stable night, and the simulated and observed boundary layers are again both dominated by sinking motion (not shown). The simulated NBL lies within the E (stable) category of the Pasquill-Gifford scale (-0.5 °C/100 m $< \Delta T/\Delta z <$ 1.5 °C/100 m), while the observed values are within the stronger F category (1.5 °C/100 m $< \Delta T/\Delta z <$ 4.0 °C/100 m). This is likely due to inadequate surface cooling in the simulation.

Similar to night 1, the HYSPLIT model is run for the tracer release from the most distant point—in this case, point UE (Fig. 2) and a release rate of 396 g/h. The cross-sections (Fig. 10b) show the plume spreading out with time, with weaker upward mixing. The plume has not yet arrived at 0700 UTC (3:00 am EDT), reaches its maximum at 0900 UTC, and starts to fade soon after. The simulated maximum values along the arc reach values similar to the observed values at the observed peak time times (Fig. 11b), again indicating that the model is adequately simulating vertical mixing.

As for night 1, 100,000 particles are released from the 329-m level of the tower, and this is used to calculate the night 2

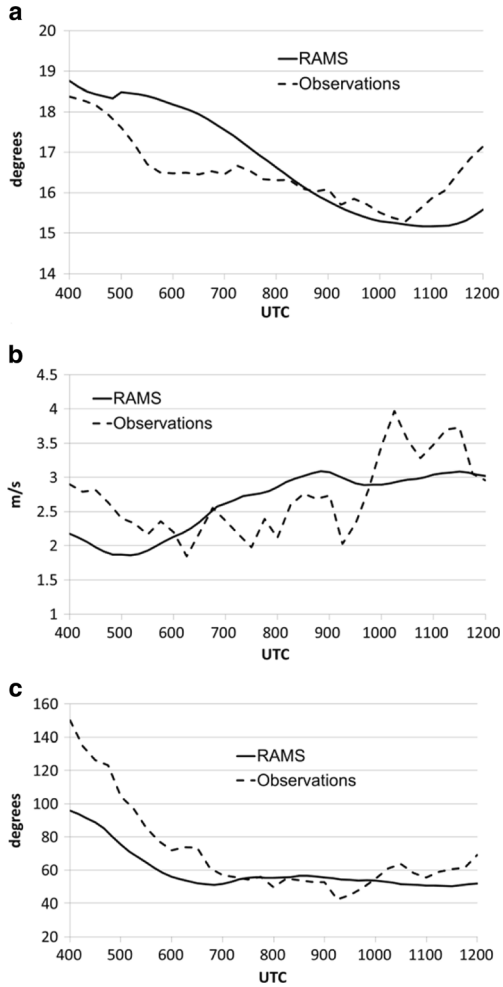

Fig. 13 Comparison of RAMS data with observed tower data for night 2 at 34 m for **a** temperature, **b** wind speed, and **c** wind direction

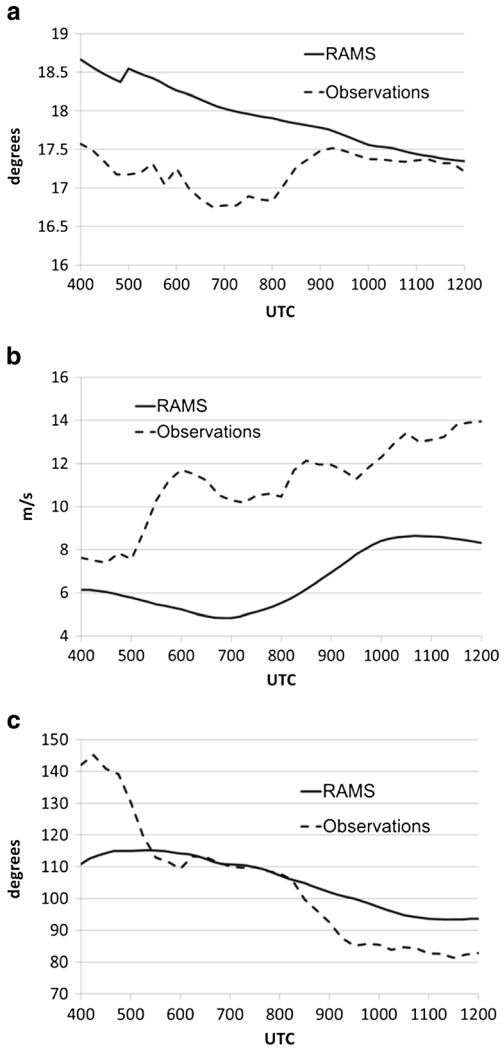

Fig. 14 As in Fig. 13 but at 329 m

footprint (Fig. 16). Early in the simulated period at 2:00 am to 3:00 am EDT (0600 to 0700 UTC), the footprints indicate a local influence comparable to night 1 (Fig. 16a, b), as the strongest inversion has not yet formed (Fig. 15b), in agreement with the generally higher boundary layer values (Fig. 1c) at this time. As night 2 progresses, however, the turbulent activity actually increases as the jet forms (Fig. 15b), as buoyant damping and dissipation are balanced by shear production, also seen in observed TKE budgets (Duarte et al. 2015). This is in agreement with Fig. 1b—the friction velocity values on night 2 rise after 0600 UTC (2:00 am EDT) until 1100 UTC when they are approximately equal between night 1 and night 2, despite the greater stability on night 2. Consequently, the footprints indicate a stronger local influence on the tower later in the night on night 2 (not seen in the tracer data, as the release was stopped at 0915 UTC). The tower is sampling an area further from the tower on night 2, however, as the footprint extends well beyond the grid 4 domain, with a large fraction of particles (70–80 %) released after 0800 UTC having left the domain after 1 h (and more than 97 % leaving after 2 h). The fraction of particles that reach the 20-m level after 1 h varies between 0.5 and 2.5 %.

As for night 1, a second release experiment is done with the particles released from the 34-m level of the tower. Now, 3–8 % of the particles have dispersed below the 20-m level within 1 h—several times more than for the 329-m release but still indicative of a small local influence.

4 Discussion and conclusions

Night 1 was characterized by a period of stronger mixing from 0600 UTC to 0900 UTC, followed by a reduction as the values of u^* and the boundary layer height both fell. The

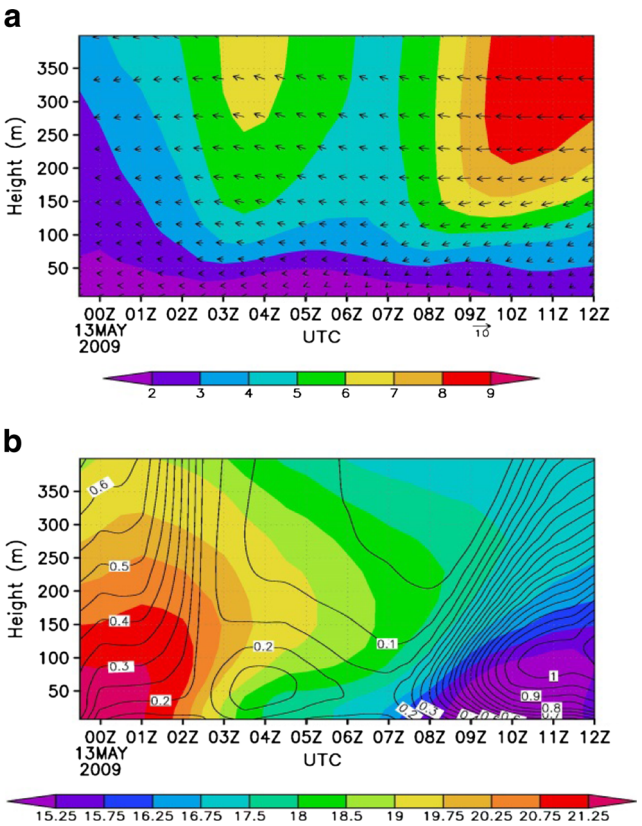

Fig. 15 As in Fig. 9 but for night 2

simulated night 1 footprints show a fading of the local influence during that latter period. Night 2 had lower values of u^* during the tracer release period and a more rapid stabilization. A period of stronger mixing beneath the jet between 0900 UTC and 1100 UTC on night 2 allowed for a larger simulated footprint during this time.

We can draw three conclusions from this experiment:

i). A tracer released within 24 km of the SCT was detected at the uppermost sensor (329 m) on the two nights, indicating that, even in nocturnal conditions, sufficient vertical mixing exists to move tracer from the surface to this level. This implies that moderately or slightly stable nocturnal conditions do not necessarily confine gases released at the surface within a shallow layer.

ii). A fetch of 25 km in length is adequate for a tracer to be mixed upwards to 329 m, a level typical of a "tall" sampling tower. This indicates that such a tower is at least partly influenced by the local landscape during a time when it is assumed to be sampling continental-scale air masses.

iii). The small χ/Q values and the simulation of the tracer release show how, while it is detectable, the local influence is small. In the backtracking simulations, only about 1–3 % of the particles at 329 m land within the domain on either night (about double that when released at 34 m), with most of the released particles leaving the domain (~20 km) within a short time (1–2 h). This suggests that the boundary layer height in Fig. 1c can be considered as a "leaky" barrier to upward diffusion, confining most of the tracer released beneath it. The fact that most particles released at 329 m ultimately left the local domain implies that this level of the tall tower is instead sampling CO_2 released hours earlier from areas beyond 25 km, as necessary to accomplish the goals of Carbon Tracker. This is similar to the conclusion from Sogachev and Leclerc (2011), in which calculated tower footprints in stable conditions often lay entirely beyond 50 km of the tower, indicating that the tower is predominately sampling areas hundreds of kilometers away.

Confidence in the results based on a simulation is of course limited by the quality of the simulation. Our simulation of the boundary layer on the two nights is in general agreement with the observed boundary layer. Errors in the simulated winds do lead to problems in the simulated plumes when compared to tracer data—on both nights, the plumes seem to form properly but not move as observed. Because the maximum simulated concentrations at the tower distance at the different tower levels are in (again, rough) agreement with the observed values, however, the simulated vertical diffusion and the simulated footprints are a good representation of the influence of the surrounding area on the tower. This conclusion is strengthened by the agreement between the simulated footprint behavior and the observed measures of stability and vertical transport.

This study has implications beyond a single tower. Our results speak to the importance of vertical transport on the calculation of a global carbon budget constrained with limited carbon measurements. Gerbig et al. (2009) discuss that errors in the parameterized vertical transport in transport models used for top-down inversions can produce errors in the reconstructed global emissions. Peters et al. (2004) demonstrated errors in the global budget of an artificial tracer (SF6) and attributed some of them to problems with the calculation of vertical eddy diffusivity in the TM5 transport model, the same model used by Carbon Tracker to get the global carbon inversion. Gerbig et al. (2009) also suggest "adding Lidar measurements to monitor mixing heights at the tall tower locations, which when assimilated into the meteorological transport fields are likely to improve the representation of the measurements." In the absence of

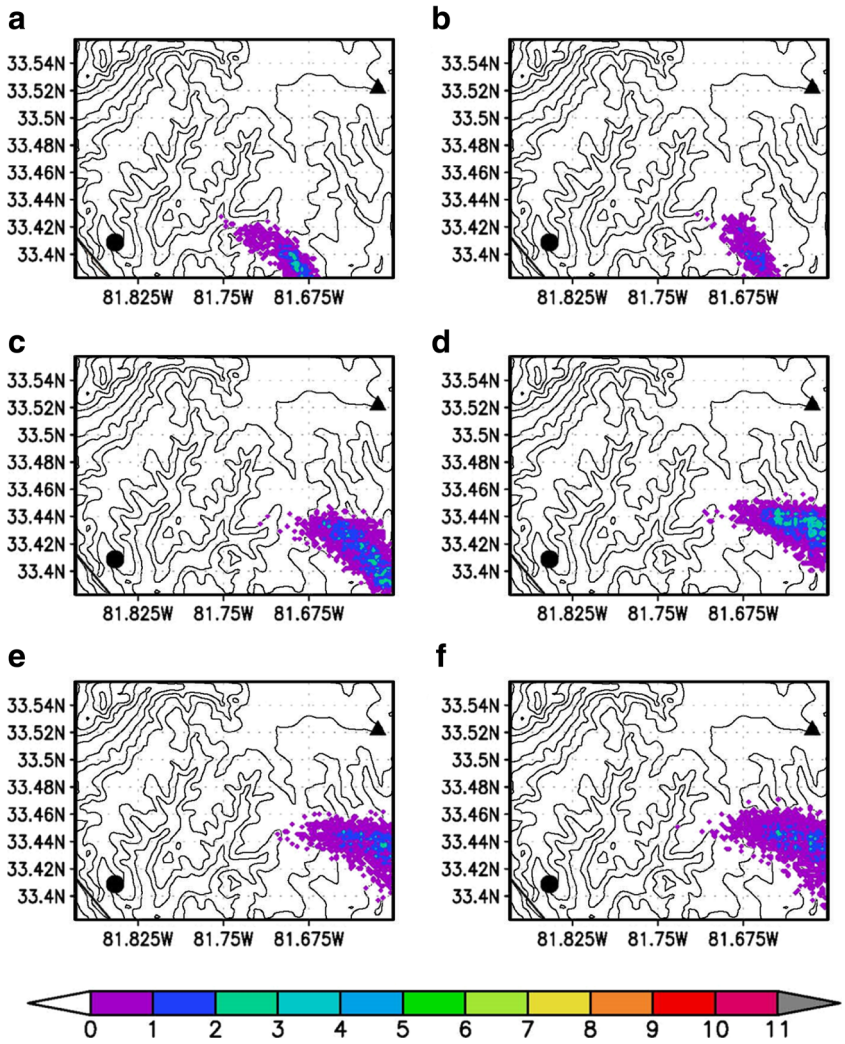

Fig. 16 As in Fig. 12 but for night 2

such measurements, numerical modeling can serve as a good proxy for the determination of mixing parameters.

We have demonstrated the benefit of modeling in assessing a tower sampling site, and this could be applied to other sites as Gerbig et al. (2009) suggests. The influence of the local environment is related to both vertical mixing and advection, and weaker advection of air from distant sources could make the local influence stronger than was seen during the nights of the tracer release. The local effect must be considered when data from a tall tower is being evaluated.

Acknowledgments This document was prepared by members of the Savannah River National Laboratory (SRNL) in conjunction with work accomplished under Contract No. DE-AC09-08SR22470 with the U.S. Department of Energy. Funding support was provided to SRNL, the University of Georgia and Brookhaven National Laboratory by the DOE Office of Science – Terrestrial Carbon Processes program.

Compliance with ethical standards

References

Andrews A, Kofler J, Trudeau M, Williams J, Neff D, Masarie K, Chao D, Kitzis D, Novelli P, Zhao C, Dlugokencky E, Lang P, Crotwell M, Fischer M, Parker M, Lee J, Baumann D, Desai A, Stanier C, de Wekker S, Wolfe D, Munger J, Tans P (2013) CO_2, CO and CH_4 measurements from the NOAA Earth System Research Laboratory's Tall Tower Greenhouse Gas Observing Network: instrumentation, uncertainty analysis and recommendations for future high-accuracy greenhouse gas monitoring efforts. Atmos Meas Techn 6:1461–1553

Barcza Z, Kern A, Haszpra L, Kljun N (2009) Spatial representativeness of tall tower eddy covariance measurements using remote sensing and footprint analysis. Agric For Meteorol 149:795–807

Barkhatov Y, Belolipetsky P, Degermendzhi A, Belolipetskii V, Verkhovets S, Timokhina A, Panov A, Shchemel A, Vedrova E, Trephilova O (2012) Modeling of CO_2 fluxes between atmosphere and boreal forest. Procedia Environ Sci 13:621–625

Benjamin S, Dévényi D, Weygandt S, Brundage K, Brown J, Grell G, Kim D, Schwartz B, Smirnova T, Smith T, Manikin G (2004) An hourly assimilation–forecast cycle: the RUC. Mon Wea Rev 132: 495–518

Birdsey R, Bates N, Behrenfeld M, Davis K, Doney S, Feely R, Hansell D, Heath L, Kasischke E, Khesghi H, Law B, Lee C, McGuire A, Raymond P, Tucker C (2009) Carbon cycle observations: gaps threaten climate mitigation policies. Eos 90(34):292–293

Chang J, Franzese P, Chayantrakom K, Hanna S (2003) Evaluations of CALPUFF, HPAC, and VLSTRACK with two mesoscale field datasets. J Appl Meteor 42:453–466

Chen B, Zhang H, Coops N, Fu D, Worthy D, Xu G, Black T (2013) Assessing scalar concentration footprint climatology and land surface impacts on tall-tower CO_2 concentration measurements in the boreal forest of central Saskatchewan, Canada. Theor Appl Clim. doi:10.1007/s00704-013-1038-2

Clark T, Hall W (1991) Multi-domain simulations of the time dependent Navier-Stokes equations: benchmark error analysis of some nesting procedures. J Comput Phys 92:456–481

Cotton W, Tripoli G, Rauber R, Mulvihill E (1986) Numerical simulation of the effects of varying ice crystal nucleation rates and aggregation processes on orographic snowfall. J Clim Appl Meteorol 25:1658–1680

Desai A, Noormets A, Bolstad P, Chen J, Cook B, Davis K, Euskirchen E, Gough C, Martin J, Ricciuto D, Schmid H, Tang J, Wang W (2008) Influence of vegetation and seasonal forcing on carbon dioxide fluxes across the Upper Midwest, USA: implications for regional scaling. Agric For Meteorol 148:288–308

Draxler R, Hess G (1998) An overview of the HYSPLIT_4 modeling system of trajectories, dispersion, and deposition. Aust Meteorol Mag 47:295–308

Duarte H, Leclerc M, Zhang G, Durden D, Kurzeja R, Parker M, Werth D (2015) Impact of nocturnal low-level jets on near-surface turbulence kinetic energy. Bound-Layer Meteorol. doi:10.1007/s10546-015-0030-z

Gerbig C, Dolman A, Heimann M (2009) On observational and modelling strategies targeted at regional carbon exchange over continents. Biogeosciences 6:1949–1959. doi:10.5194/bg-6-1949-2009

Gloor M, Bakwin P, Hurst D, Lock L, Draxler R, Tans P (2001) What is the concentration footprint of a tall tower? J. Geophys Res 106: 17831–17840

Gourdji S, Mueller K, Yadav V, Huntzinger D, Andrews A, Trudeau M, Petron G, Nehrkorn T, Eluszkiewicz J, Henderson J, Wen D, Lin J, Fischer M, Sweeney C, Michalak A (2012) North American CO_2 exchange: inter-comparison of modeled estimates with results from a fine-scale atmospheric inversion. Biogeosciences 9:457–475. doi:10.5194/bg-9-457-2012

Harrington J (1997) The effects of radiative and microphysical processes on simulated warm transition season Arctic stratus, Dept. of Atmospheric Science Bluebook 637, Colorado State University, Fort Collins, CO, 289 pp.

Hegarty J et al. (2013) Evaluation of Lagrangian particle dispersion models with measurements from controlled tracer releases. J Appl Meteorol Climatol 52:2623–2637. doi:10.1175/JAMC-D-13-0125.1

Hsieh C-I, Katul G, Chi T (2000) An approximate analytical model for footprint estimation of scalar fluxes in thermally stratified atmospheric flows. Adv Water Resour 23:765–772

Kuo H (1974) Further studies of the parameterization of the influence of cumulus convection on large-scale flow. J Atmos Sci 31:1232–1240

Leclerc M, Karipot A, Prabha T, Allwine G, Lamb B, Gholz H (2003a) Impact of non-local advection on flux footprints over a tall forest canopy: a tracer flux experiment. Agric For Meteorol 115:19–30

Leclerc M, Meskhidze N, Finn D (2003b) Comparison between measured tracer fluxes and footprint model predictions over a homogeneous canopy of intermediate roughness. Agric For Meteorol 117:145–158

Mellor G, Yamada T (1974) A hierarchy of closure models for planetary boundary layers. J Atmos Sci 31:1791–1806

Mesinger F, Arakawa A (1976) Numerical methods used in atmospheric models. GARP Publication Series, No. 14, WMO/ICSU Joint Organizing Committee, 64pp.

Mesinger F, DiMego G, Kalnay E, Shafran P, Ebisuzaki W, Jovic D, Woollen J, Mitchell K, Rogers E, Ek M, Fan Y, Grumbine R, Higgins W, Li H, Lin Y, Manikin G, Parrish D, Shi W (2004) North American Regional Reanalysis. 15th Symposium on Global Change and Climate Variations, paper P1.1, Combined Preprints CD-ROM, 84th AMS Annual Meeting, Seattle, WA. Updated 31 December 2003

Meyers M, DeMott P, Cotton W (1992) New primary ice nucleation parameterizations in an explicit cloud model. J Appl Meteorol 31: 708–721

Pasquill F, Smith F (1983) Atmospheric diffusion. Wiley, NY

Perry S, Cimorelli A, Paine R, Brode R, Weil J, Venkatram A, Wilson R, Lee R, Peters W (2005) AERMOD: a dispersion model for industrial source applications. Part II: model performance against 17 field study databases. J Appl Meteorol 44:694–708

Peters W, Jacobson A, Sweeney C, Andrews A, Conway T, Masarie K, Miller J, Bruhwiler L, Pétron G, Hirsch A, Worthy D, van der Werf G, Randerson J, Wennberg P, Krol M, Tans P (2007) An atmospheric perspective on North American carbon dioxide exchange: CarbonTracker. Proc Natl Acad Sci U S A 104(48):18925–18930. doi:10.1073/pnas.0708986104

Peters W, Krol M, Dlugokencky E, Dentener F, Bergamaschi P, Dutton G, Velthoven P, Miller J, Bruhwiler L, Tans P (2004) Toward regional-scale modeling using the two-way nested global model TM5: characterization of transport using SF_6. J Geophys Res 109:D19314. doi:10.1029/2004JD005020

Pielke R, Cotton W, Walko R, Tremback C, Lyons W, Grasso L, Nicholls M, Moran M, Wesley D, Lee T, Copeland J (1992) A comprehensive meteorological modeling system-RAMS. Meteorol Atmos Phys 49: 69–91

Schmid H (2002) Footprint modeling for vegetation atmosphere exchange studies: a review and perspective. Agric For Meteorol 113: 159–183

Smagorinsky J (1963) General circulation experiments with the primitive equations. Part I. The basic experiment. Mon Weather Rev 91:99–164

Sogachev A, Leclerc M (2011) On concentration footprints for a tall tower in the presence of a nocturnal low-level jet. Agric For Meteorol 151:755–764

Stephens B, Gurney K, Tans P, Sweeney C, Peters W, Bruhwiler L, Ciais P, Ramonet M, Bousquet P, Nakazawa T, Aoki S, Machida T, Inoue G, Vinnichenko N, Lloyd J, Jordan A, Heimann M, Shibistova O, Langenfelds R, Steele L, Francey R, Denning A (2007) Weak northern and strong tropical land carbon uptake from vertical profiles of atmospheric CO_2. Science 316(5832):1732–1735. doi:10.1126/science.1137004

Stunder B, Heffter J, Draxler R (2007) Airborne volcanic ash forecast area reliability. Weather Forecast 22:1132–1139

van Dop H, Addis R, Fraser G, Girardi F, Graziani G, Inoue Y, Kelly N, Klug W, Kulmala A, Nodop K, Pretel J (1998) ETEX: a European

tracer experiment; observations, dispersion modelling and emergency response. Atmos Environ 32:4089–4094

Walko R, Band L, Baron J, Kittel T, Lammers R, Lee T, Ojima D, Pielke R, Taylor C, Tague C, Tremback C, Vidale P (2000) Coupled atmosphere–biophysics–hydrology models for environmental modeling. J Appl Meteorol 39:931–944

Wang W, Davis K, Cook B, Yi C, Butler M, Ricciuto D, Bakwin P (2007) Estimating daytime CO2 fluxes over a mixed forest from tall tower mixing ratio measurements. J Geophys Res V112, 2006JD007770

Werth D, Kurzeja R, Luís Dias N, Zhang G, Duarte H, Fischer M, Parker M, Leclerc M (2011) The simulation of the southern great plains nocturnal boundary layer and the low-level jet with a high-resolution mesoscale atmospheric model. J Appl Meteorol Climatol 50:1497–1513